Supplementary Information (SI) for Inorganic Chemistry Frontiers.

SUPPORTING INFORMATION

Role of M-site cation in The Negative Linear Compressibility of Rutile-Like $M^{II}(dca)_2$

Muzi Chen,*[abc] Hanna L. B. Boström,[de] Dominik Daisenberger,[f] and Andrew B. Cairns*[ab]

[a] Department of Materials, Imperial College London, Royal School of Mines,

Exhibition Road, SW7 2AZ, London, U.K

[b] London Centre for Nanotechnology, Imperial College London, London SW7 2AZ, UK

[c] Department of Heterogeneous Catalysis, Max-Planck-Institut für Kohlenforschung,

Kaiser-Wilhelm-Platz 1, 45470 Mülheim an der Ruhr, Germany

[d] Department of Chemistry, Stockholm University, Svante Arrhenius väg 16C, SE-106 91, Stockholm, Sweden

[e] Wallenberg Initiative Materials Science for Sustainability, Department of Chemistry, Stockholm University, SE-114 18, Stockholm, Sweden

[f] Diamond Light Source Ltd., Harwell Campus, Didcot OX11 0DE, U.K

∗To whom correspondence should be addressed;

E-mail: muzichen@kofo.mpg.de

E-mail: a.cairns@imperial.ac.uk

Contents

1. Bulk modulus and linear compressibility

Table S1: Compressibility and bulk modulus of $Ni(dca)_2$, $Mn(dca)_2$, and $Fe(dca)_2$ calculated within different pressure ranges.

Materials	K_a (TPa^{-1})	K_b (TPa^{-1})	K_c (TPa^{-1})	B_0 (GPa)	B'	Range (GPa)	Data points
LP-$Ni(dca)_2$	35.7(12)	13.1(5)	-2.5 (8)	17.9(4)	4	0.07 – 1.06	13
HP-$Ni(dca)_2$	18.8(10)	17.8(6)	9.4(7)	15.9(4)	4	1.21 – 3.16	22
LP-$Mn(dca)_2$	34(8)	20(2)	-10(3)	18.2(7)	4	0.04 – 0.30	5
HP-$Mn(dca)_2$	17.9(15)	26.6(13)	10.4(12)	9.6(2)	4	0.44 – 2.78	16
LP-$Fe(dca)_2$	40(3)	16.8(7)	-2.8(4)	14.9(4)	4	0.03 – 0.95	13
HP-$Fe(dca)_2$	34(5)	38(3)	18(4)	14.6(7)	0.2(3)	1.11 – 2.44	8

2. Crystallographic details

Table S2: Crystallographic details determined by Rietveld refinement of X-ray diffraction data for $Ni(dca)_2$ at 0.07 GPa.

Space group	*Pnnm*
a / Å	5.9568(5)
b / Å	7.0006(6)
c / Å	7.2912(10)
β/ °	90
V / $Å^3$	304.05(6)
R_{wp}	0.98%

Atom	**occ**	***x***	***y***	***z***	**B_{iso}* / $Å^2$**
C	1	0.237(4)	0.342(4)	0.158(3)	0.9(3)
Ni	1	0	0	0	0.9(3)
N1	1	0.292(3)	0.404(3)	0.296(2)	0.9(3)
N2	1	0.173(5)	0.269(4)	0	0.9(3)

* B_{iso} constrained to be equal for all atoms.

Table S3: Crystallographic details determined by Rietveld refinement of X-ray diffraction data for $Ni(dca)_2$ at 1.49 GPa.

Space group	*$P2_1/n$*
a / Å	5.6738(8)
b / Å	6.8548(11)
c / Å	7.317(2)
β/ °	92.818(11)
V / $Å^3$	284.24(10)
Rwp	0.85%

Atom	**occ**	***x***	***y***	***z***	**Biso* / $Å^2$**
C1	1	0.232(10)	0.145(11)	0.292(9)	2.1(5)
C2	1	-0.256(13)	-0.138(8)	0.361(9)	2.1(5)
Ni	1	0.5	0	0	2.1(5)
N1	1	0.266(8)	0.108(7)	0.176(6)	2.1(5)
N2	1	0.174(9)	0.206(6)	0.481(7)	2.1(5)
N3	1	-0.264(7)	-0.086(6)	0.205(7)	2.1(5)

* B_{iso} constrained to be equal for all atoms.

Table S4: Crystallographic details determined by Rietveld refinement of X-ray diffraction data for $Mn(dca)_2$ at 0.04 GPa.

Space group	*Pnnm*
a / Å	6.1352(9)
b / Å	7.3046(9)
c / Å	7.5317(12)
β/ °	90
V / $Å^3$	337.53(8)
R_{wp}	0.88%

Atom	**occ**	***x***	***y***	***z***	**B_{iso}* / $Å^2$**
C	1	0.238(12)	0.356(5)	0.181(4)	3.3(6)
Mn	1	0	0	0	3.3(6)
N1	1	0.276(7)	0.387(4)	0.291(3)	3.3(6)
N2	1	0.177(8)	0.304(5)	0	3.3(6)

* B_{iso} constrained to be equal for all atoms.

Table S5: Crystallographic details determined by Rietveld refinement of X-ray diffraction data for $Mn(dca)_2$ at 0.85 GPa.

Space group	*$P2_1/n$*
a / Å	5.893(2)
b / Å	7.154(3)
c / Å	7.518(3)
β/ °	95.31(3)
V / $Å^3$	315.6(2)
Rwp	0.90%

Atom	**occ**	***x***	***y***	***z***	**Biso* / $Å^2$**
C1	1	0.20(3)	0.14(2)	0.28(2)	13(3)
C2	1	0.00(4)	0.08(2)	0.30(2)	13(3)
Mn	1	0.5	0	0	13(3)
N1	1	0.328(12)	0.14(2)	0.134(15)	13(3)
N2	1	0.12(2)	0.14(2)	0.37(2)	13(3)
N3	1	-0.20(2)	-0.013(11)	0.19(2)	13(3)

* B_{iso} constrained to be equal for all atoms.

Table S6: Crystallographic details determined by Rietveld refinement of X-ray diffraction data for $Fe(dca)_2$ at 0.05 GPa.

Space group	*Pnnm*
a / Å	6.072(3)
b / Å	7.152(3)
c / Å	7.429(3)
β/ °	90
V / $Å^3$	322.6(2)
R_{wp}	0.60%

Atom	**occ**	***x***	***y***	***z***	**B_{iso}* / $Å^2$**
C	1	0.207(7)	0.354(6)	0.146(3)	5.6(8)
Fe	1	0	0	0	5.6(8)
N1	1	0.269(5)	0.391(4)	0.268(2)	5.6(8)
N2	1	0.135(11)	0.309(7)	0	5.6(8)

* B_{iso} constrained to be equal for all atoms.

Table S7: Crystallographic details determined by Rietveld refinement of X-ray diffraction data for $Fe(dca)_2$ at 2.01 GPa.

Space group	*$P2_1/n$*
a / Å	5.707(5)
b / Å	6.937(4)
c / Å	7.450(6)
β/ °	95.40(8)
V / $Å^3$	293.7(4)
Rwp	0.46%

Atom	**occ**	***x***	***y***	***z***	**Biso* / $Å^2$**
C1	1	0.21(2)	0.151(11)	0.311(14)	11(2)
C2	1	-0.042(2)	0.079(13)	0.228(15)	11(2)
Fe	1	0.5	0	0	11(2)
N1	1	0.366(9)	0.145(8)	0.222(10)	11(2)
N2	1	0.048(14)	0.158(9)	0.399(14)	11(2)
N3	1	-0.176(10)	-0.039(10)	-0.030(9)	11(2)

* B_{iso} constrained to be equal for all atoms.

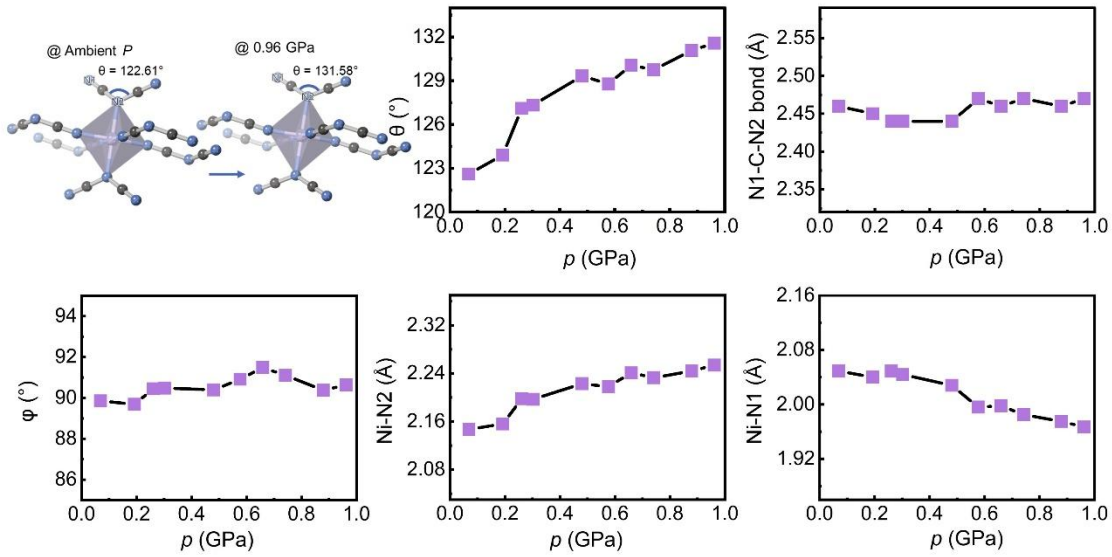

Figure S1. Pressure-induced structural deformation in $Ni(dca)_2$. Top left: Local coordination environment showing the dca^- ligand geometry at ambient pressure (θ = 122.61°) and at 0.96 GPa (θ = 131.58°), where θ represents the C–N2–C bond angle. The graphs show the evolution with pressure of: (top center) the C–N2–C angle θ in the dca^- ligand, (top right) the N1–C–N2 bond length, (middle left) the octahedral distortion parameter $\phi = |\phi' - 90°|$, (middle right) the Ni–N2 bond length, and (bottom) the Ni–N1 bond length. All structural parameters were obtained from Rietveld refinement of high-pressure powder X-ray diffraction data. The dashed lines serve as guides to the eye. Error bars are within the size of the data points where not visible.

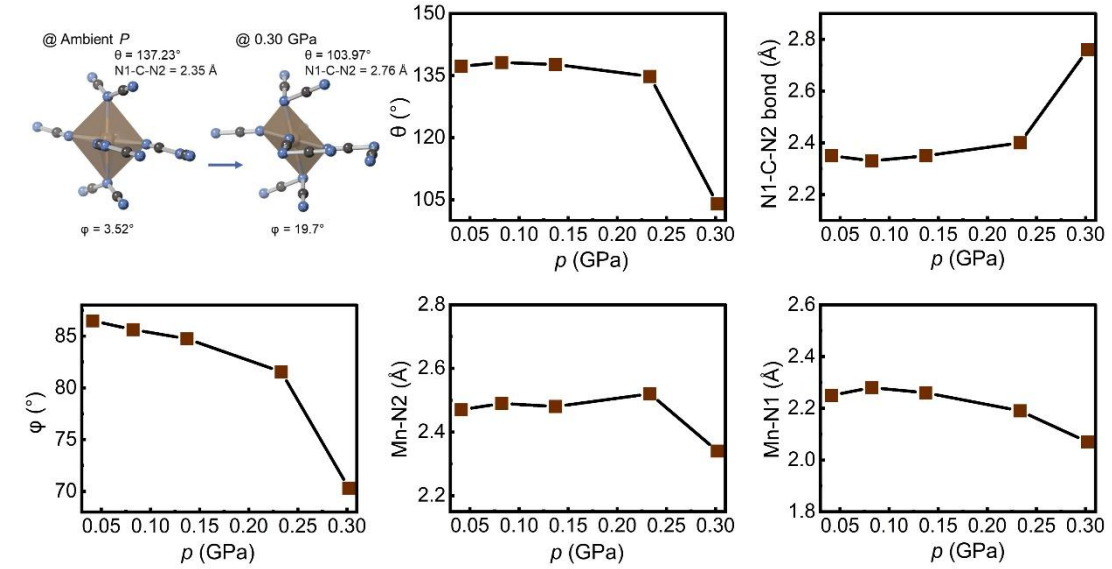

Figure S2. Pressure-induced structural deformation in $Mn(dca)_2$. Top left: Local coordination environment showing the dca^- ligand geometry and octahedral distortion at ambient pressure (θ = 137.23°, N1-C-N2 = 2.35 Å, ϕ = 3.52°) and at 0.30 GPa (θ = 103.97°, N1-C-N2 = 2.76 Å, ϕ = 19.7°), where θ represents the C–N2–C bond angle and ϕ quantifies the octahedral distortion. The graphs show the evolution with pressure

of: (top center) the C–N2–C angle θ in the dca^- ligand, (top right) the N1–C–N2 bond length, (bottom left) the octahedral distortion parameter ϕ = |ϕ' − 90°|, (bottom center) the Mn–N2 bond length, and (bottom right) the Mn–N1 bond length. All structural parameters were obtained from Rietveld refinement of high-pressure powder X-ray diffraction data. The dashed lines serve as guides to the eye. Error bars are within the size of the data points where not visible.

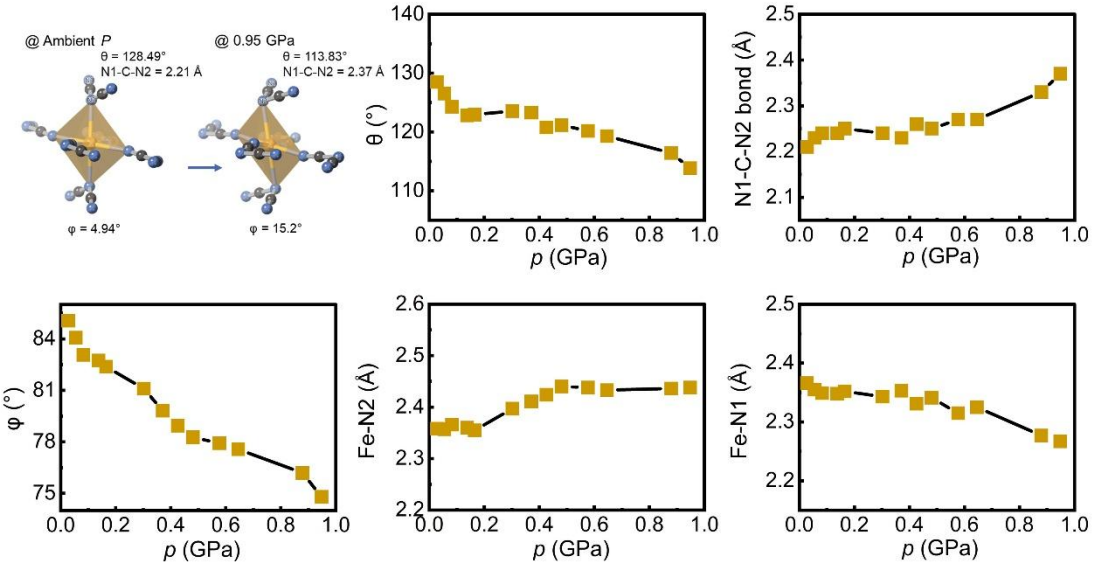

Figure S3. Pressure-induced structural deformation in $Fe(dca)_2$. Top left: Local coordination environment showing the dca^- ligand geometry and octahedral distortion at ambient pressure (θ = 128.49°, N1-C-N2 = 2.21 Å, ϕ = 4.94°) and at 0.95 GPa (θ = 113.83°, N1-C-N2 = 2.37 Å, ϕ = 15.2°), where θ represents the C–N2–C bond angle and ϕ quantifies the octahedral distortion. The graphs show the evolution with pressure of: (top center) the C–N2–C angle θ in the dca^- ligand, (top right) the N1–C–N2 bond length, (middle left) the octahedral distortion parameter ϕ = |ϕ' − 90°|, (middle right) the Fe–N2 bond length, and (bottom right) the Fe–N1 bond length. All structural parameters were obtained from Rietveld refinement of high-pressure powder X-ray diffraction data. The dashed lines serve as guides to the eye. Error bars are within the size of the data points where not visible.

3. Variable-pressure X-ray diffraction data of $Ni(dca)_2$

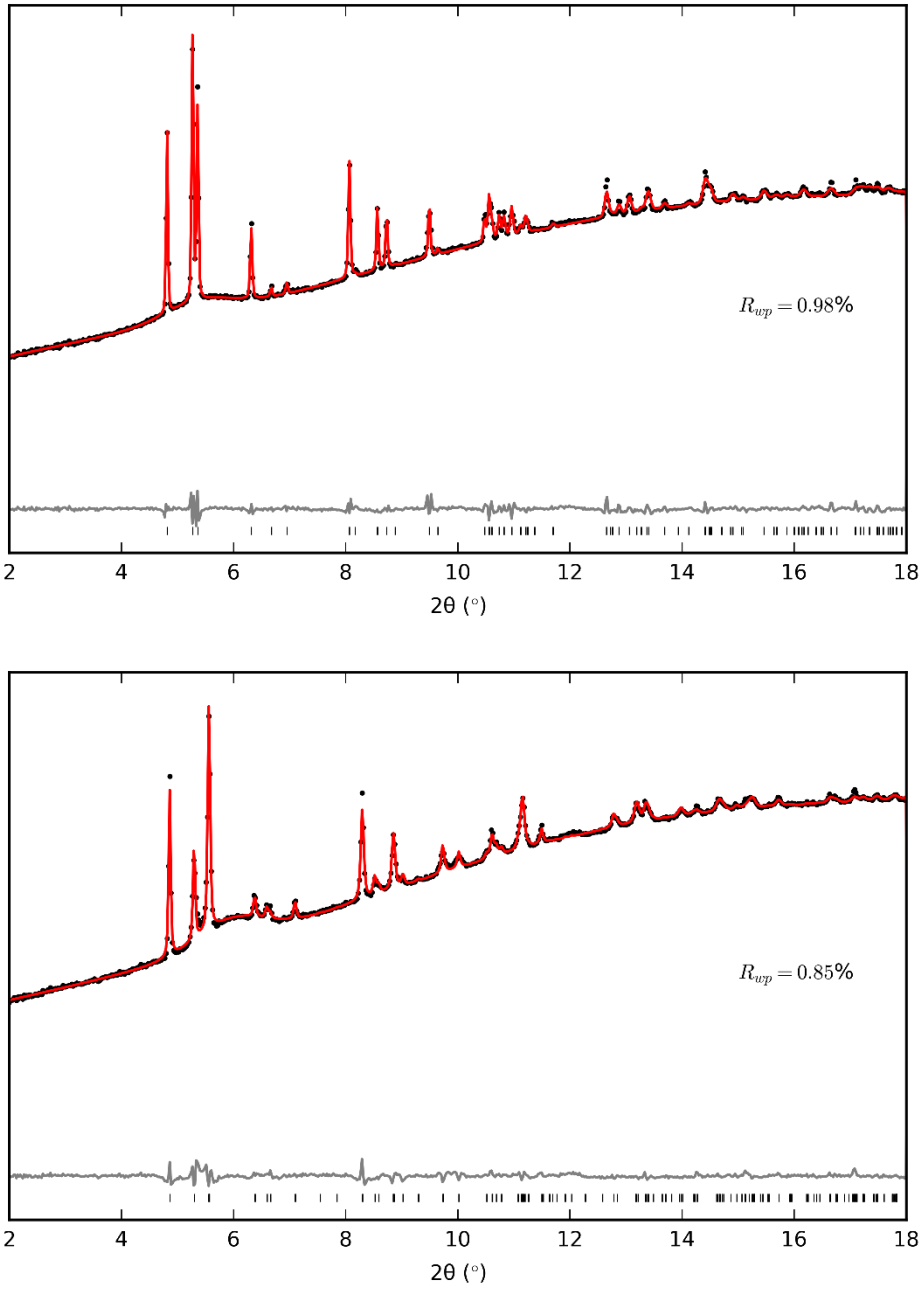

Figure S4: Powder X-ray diffraction patterns of the orthorhombic (top) and monoclinic (bottom) phases of $Ni(dca)_2$ at 0.07 GPa and 1.49 GPa, respectively. Data were measured at Diamond Light Source (I15) using radiation with a wavelength of 0.4246 Å. They were fitted using Rietveld refinement. The experimental data are displayed in black, the fit in red, the residuals in grey, and the permitted reflections are denoted by vertical bars. The R_{wp} value is given as a satisfactory indicator of refinement.

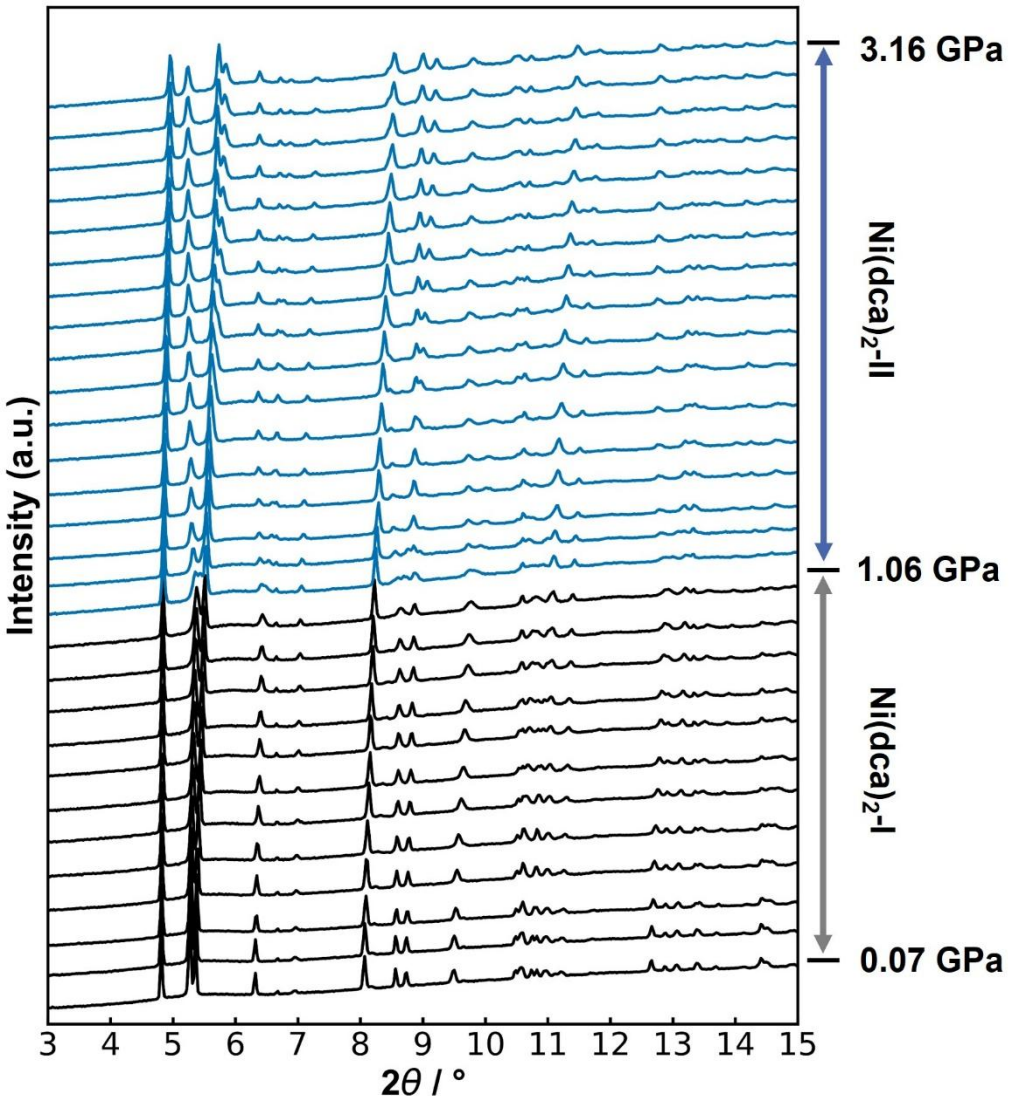

Figure S5: HP-PXRD patterns of $Ni(dca)_2$ measured at Diamond Light Source using radiation with a wavelength of 0.4246 Å. The patterns represent, in ascending order, the orthorhombic (0.07-1.06 GPa) and monoclinic (1.21-3.16 GPa) phases.

Table S8: Lattice parameters and unit cell volumes of $Ni(dca)_2$ as a function of pressure during compression. Pressure uncertainties are estimated at ±0.1 GPa or less, with smaller uncertainties for fine pressure steps.

p / GPa	Space group	*a* / Å	*b* / Å	*c* / Å	β / °	*V* / Å^3	R_{wp}
0.07	*Pnnm*	5.9568(5)	7.0006(6)	7.2912(10)	90	304.05(6)	0.98
0.19	*Pnnm*	5.9262(5)	6.9826(7)	7.2913(9)	90	301.72(6)	0.86
0.26	*Pnnm*	5.9138(6)	6.9793(7)	7.2944(11)	90	301.07(6)	0.81
0.30	*Pnnm*	5.8938(6)	6.9688(7)	7.2952(11)	90	299.64(6)	0.82
0.48	*Pnnm*	5.8612(7)	6.9550(9)	7.2986(14)	90	297.53(8)	0.82
0.58	*Pnnm*	5.8352(8)	6.9446(11)	7.300(2)	90	295.80(9)	0.94
0.66	*Pnnm*	5.8143(8)	6.9394(10)	7.3045(15)	90	294.72(8)	0.91
0.74	*Pnnm*	5.8028(9)	6.9342(11)	7.308(2)	90	294.07(9)	0.99
0.88	*Pnnm*	5.7689(9)	6.9174(12)	7.302(2)	90	291.40(10)	1.00
0.96	*Pnnm*	5.7591(10)	6.9136(13)	7.311(2)	90	291.10(11)	1.06
1.44	$P2_1/n$	5.6807(9)	6.8640(10)	7.327(2)	92.649(12)	285.40(11)	0.90
1.49	$P2_1/n$	5.6738(8)	6.8548(11)	7.317(2)	92.818(11)	284.24(10)	0.85
1.51	$P2_1/n$	5.6703(7)	6.8504(11)	7.312(2)	92.9620(12)	283.64(11)	0.83
1.60	$P2_1/n$	5.6655(8)	6.8431(11)	7.306(2)	93.216(12)	282.82(10)	0.84
1.66	$P2_1/n$	5.6526(9)	6.8326(11)	7.304(2)	93.61(10)	281.52(10)	0.81
1.75	$P2_1/n$	5.6427(9)	6.8210(11)	7.30(2)	93.914(12)	280.54(9)	0.76
1.86	$P2_1/n$	5.6310(8)	6.8044(10)	7.3096(15)	94.291(10)	279.29(8)	0.74
1.98	$P2_1/n$	5.6164(7)	6.7874(9)	7.3080(14)	94.652(9)	277.67(7)	0.68
2.11	$P2_1/n$	5.6059(7)	6.7734(9)	7.3075(14)	94.941(9)	276.44(7)	0.66
2.23	$P2_1/n$	5.5924(7)	6.7531(9)	7.3053(14)	95.2425(8)	274.74(7)	0.64
2.37	$P2_1/n$	5.5786(7)	6.7317(9)	7.2998(14)	95.5354(8)	272.85(7)	0.64
2.51	$P2_1/n$	5.5679(6)	6.7150(7)	7.2948(14)	95.756(8)	271.37(7)	0.63
2.67	$P2_1/n$	5.5597(6)	6.7004(8)	7.2944(14)	95.993(8)	270.25(7)	0.61
2.81	$P2_1/n$	5.5511(7)	6.6850(9)	7.2900(15)	96.167(8)	268.96(7)	0.60
2.92	$P2_1/n$	5.5455(7)	6.6770(12)	7.289(2)	96.271(9)	268.28(8)	0.61
3.03	$P2_1/n$	5.5402(8)	6.6655(12)	7.287(2)	96.407(10)	267.41(9)	0.61
3.16	$P2_1/n$	5.5333(8)	6.656(12)	7.283(2)	96.512(11)	266.52(9)	0.59

4. Variable-pressure X-ray diffraction data of $Mn(dca)_2$

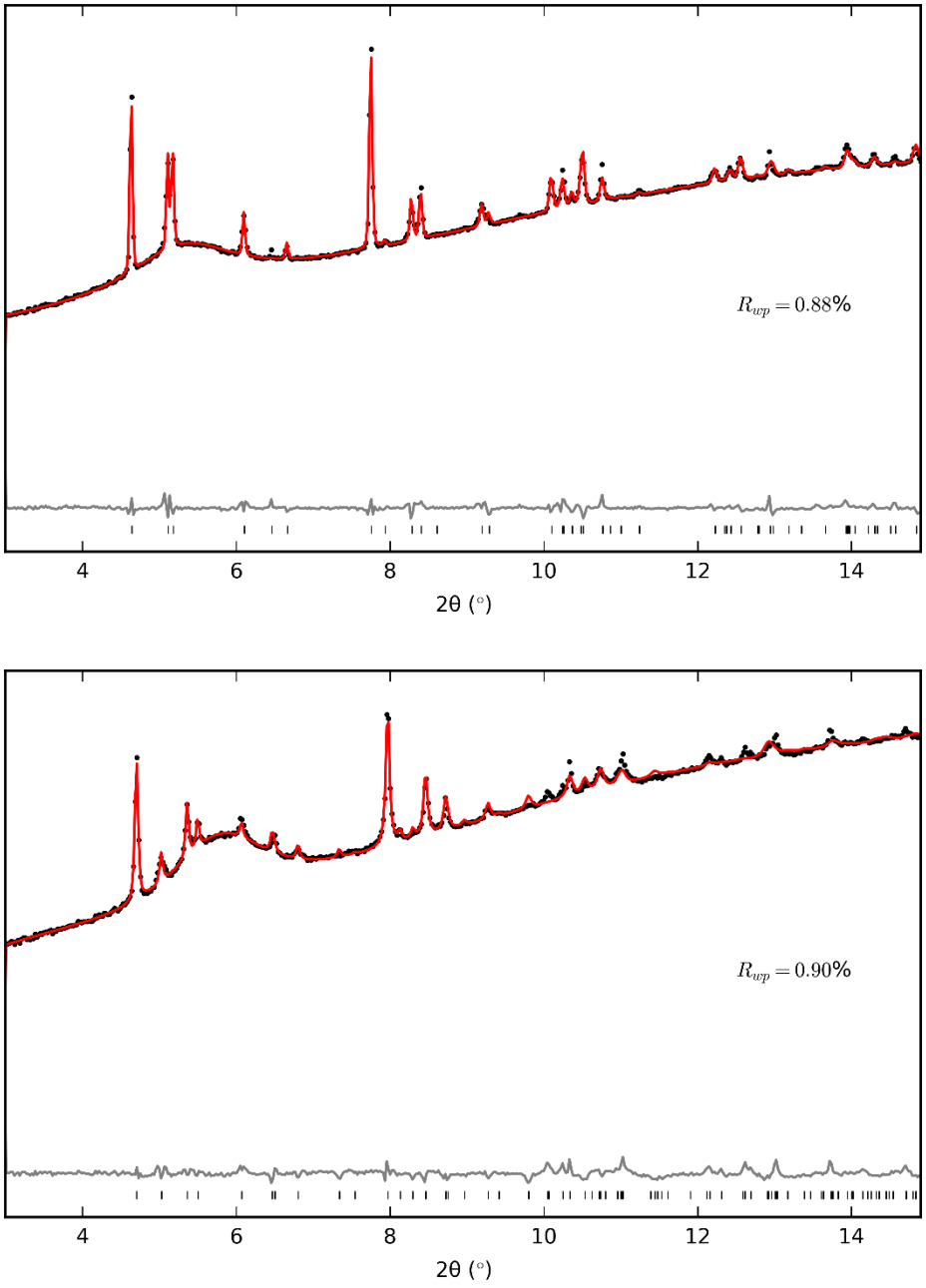

Figure S6: Powder X-ray diffraction patterns of the orthorhombic (top) and monoclinic (bottom) phases of $Mn(dca)_2$ at 0.04 GPa and 0.85 GPa, respectively. Data were measured at Diamond Light Source (I15) using radiation with a wavelength of 0.4246 Å. They were fitted using Rietveld refinement. The experimental data are displayed in black, the fit in red, the residuals in grey, and the permitted reflections are denoted by vertical bars. The R_{wp} value is given as a satisfactory indicator of refinement.

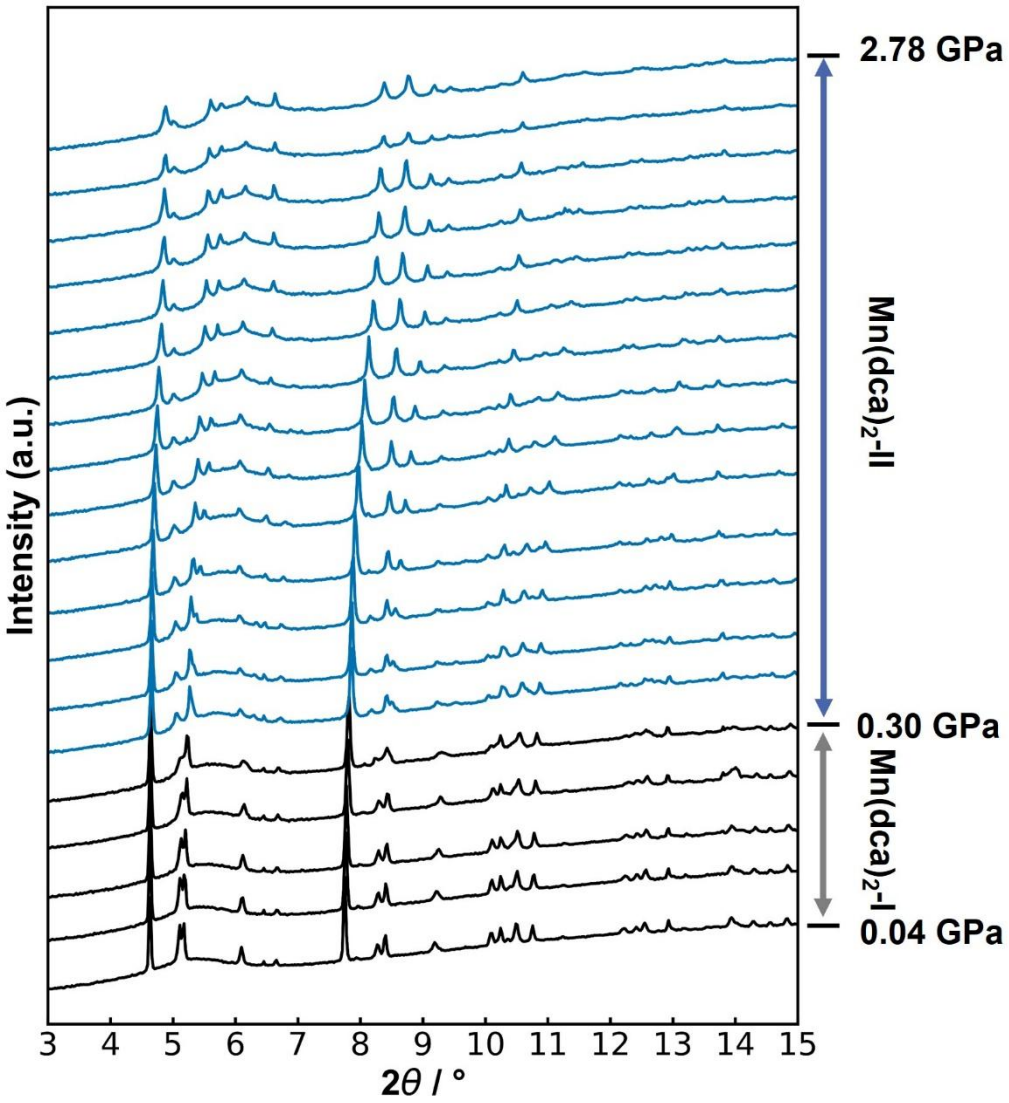

Figure S7: HP-PXRD patterns of $Mn(dca)_2$ measured at Diamond Light Source using radiation with a wavelength of 0.4246 Å. The patterns represent, in ascending order, the orthorhombic (0.04-0.3 GPa) and monoclinic (0.44-2.78 GPa) phases.

Table S9: Lattice parameters and unit cell volumes of $Mn(dca)_2$ as a function of pressure during compression. Pressure uncertainties are estimated at ±0.1 GPa or less, with smaller uncertainties for fine pressure steps.

p / GPa	Space group	*a* / Å	*b* / Å	*c* / Å	β / °	*V* / Å^3	R_{wp}
0.04	*Pnnm*	6.1352(9)	7.3046(9)	7.5317(12)	90	337.53(9)	0.88
0.08	*Pnnm*	6.1177(8)	7.3015(7)	7.5436(11)	90	336.96(8)	0.83
0.14	*Pnnm*	6.0988(11)	7.2937(8)	7.5466(14)	90	335.69(9)	0.84
0.23	*Pnnm*	6.074(2)	7.2849(13)	7.556(2)	90	334.39(15)	1.09
0.30	*Pnnm*	6.057(2)	7.271(2)	7.561(3)	90	332.9(2)	0.82
0.44	*P2$_1$/n*	5.998(5)	7.244(3)	7.531(4)	92.90(4)	326.8(3)	0.64
0.47	*P2$_1$/n*	5.985(5)	7.236(4)	7.524(4)	93.10(4)	325.4(4)	0.63
0.52	*P2$_1$/n*	5.962(4)	7.222(4)	7.530(4)	93.59(3)	323.6(3)	0.63
0.67	*P2$_1$/n*	5.9347(15)	7.193(2)	7.532(3)	94.49(2)	320.5(2)	0.97
0.85	*P2$_1$/n*	5.893(2)	7.154(3)	7.518(3)	95.31(3)	315.6(2)	0.90
1.09	*P2$_1$/n*	5.853(2)	7.099(3)	7.501(3)	96.15(2)	309.8(2)	0.77
1.22	*P2$_1$/n*	5.826(2)	7.059(3)	7.483(3)	96.64(3)	305.7(2)	0.78
1.47	*P2$_1$/n*	5.795(2)	7.000(3)	7.468(3)	97.24(3)	300.5(2)	0.64
1.82	*P2$_1$/n*	5.770(2)	6.922(3)	7.443(2)	97.76(2)	294.6(2)	0.63
2.02	*P2$_1$/n*	5.759(2)	6.872(3)	7.429(2)	98.00(2)	291.1(2)	0.60
2.05	*P2$_1$/n*	5.756(2)	6.862(3)	7.428(2)	98.04(2)	290.5(2)	0.59
2.09	*P2$_1$/n*	5.756(2)	6.855(3)	7.426(2)	98.10(2)	290.1(2)	0.58
2.16	*P2$_1$/n*	5.748(2)	6.838(3)	7.421(2)	98.14(3)	288.7(2)	0.62
2.31	*P2$_1$/n*	5.741(2)	6.813(3)	7.416(2)	98.28(3)	287.0(2)	0.59
2.53	*P2$_1$/n*	5.717(2)	6.778(4)	7.403(3)	98.41(3)	283.8(2)	0.60
2.78	*P2$_1$/n*	5.697(3)	6.764(4)	7.397(3)	98.55(4)	281.9(2)	0.59

5. Variable-pressure X-ray diffraction data of $Fe(dca)_2$

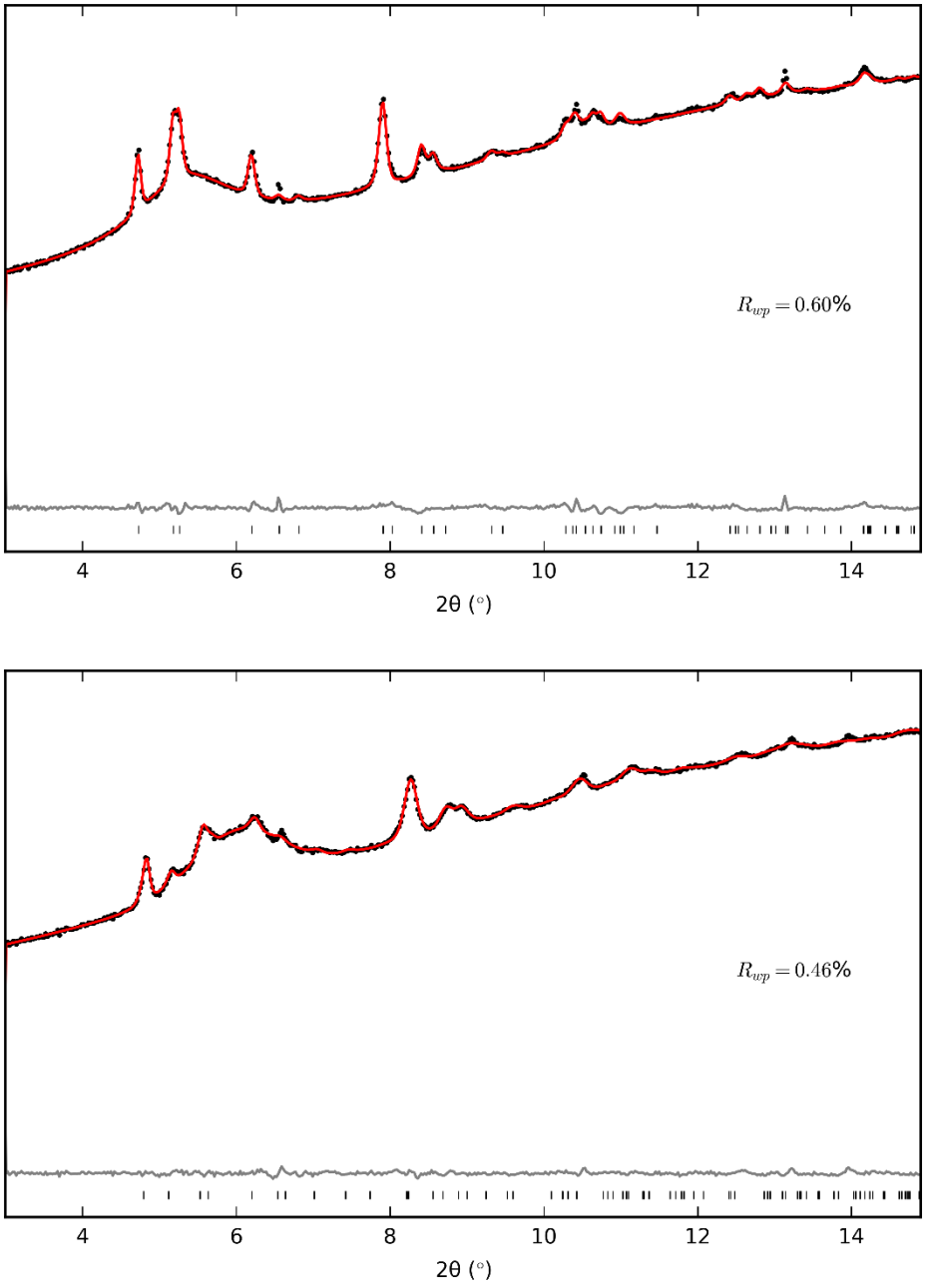

Figure S8: Powder X-ray diffraction patterns of the orthorhombic (top) and monoclinic (bottom) phases of $Fe(dca)_2$ at 0.05 GPa and 2.01 GPa, respectively. Data were measured at Diamond Light Source (I15) using radiation with a wavelength of 0.4246 Å. They were fitted using Rietveld refinement. The experimental data are displayed in black, the fit in red, the residuals in grey, and the permitted reflections are denoted by vertical bars. The R_{wp} value is given as a satisfactory indicator of refinement.

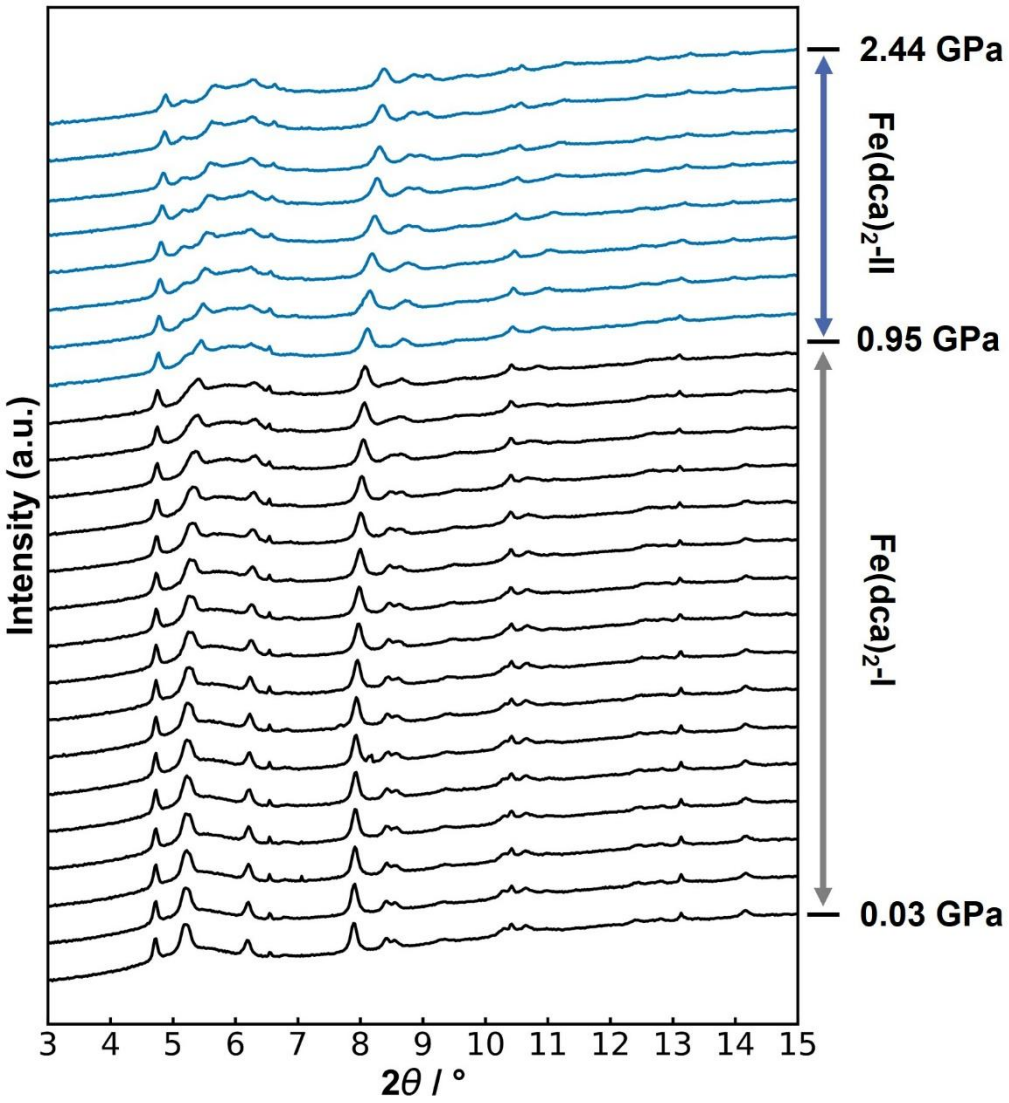

Figure S9: HP-PXRD patterns of $Fe(dca)_2$ measured at Diamond Light Source using radiation with a wavelength of 0.4246 Å. The patterns represent, in ascending order, the orthorhombic (0.03-0.95 GPa) and monoclinic (1.11-2.44 GPa) phases.

Table S10: Lattice parameters and unit cell volumes of $Fe(dca)_2$ as a function of pressure during compression. Pressure uncertainties are estimated at ±0.1 GPa or less, with smaller uncertainties for fine pressure steps.

p / GPa	Space group	*a* / Å	*b* / Å	*c* / Å	β / °	*V* / Å^3	R_{wp}
0.03	*Pnnm*	6.086(3)	7.155(3)	7.425(3)	90	323.3(2)	0.61
0.05	*Pnnm*	6.072(3)	7.152(3)	7.429(3)	90	322.6(2)	0.60
0.08	*Pnnm*	6.053(3)	7.145(3)	7.429(3)	90	321.3(2)	0.61
0.14	*Pnnm*	6.045(3)	7.140(2)	7.428(3)	90	320.6(2)	0.57
0.16	*Pnnm*	6.041(3)	7.141(2)	7.430(3)	90	320.5(2)	0.58
0.30	*Pnnm*	6.002(3)	7.124(2)	7.433(3)	90	317.8(2)	0.56
0.37	*Pnnm*	5.971(3)	7.116(3)	7.438(4)	90	316.0(3)	0.54
0.43	*Pnnm*	5.956(3)	7.108(3)	7.437(4)	90	314.9(2)	0.52
0.48	*Pnnm*	5.933(3)	7.100(3)	7.435(4)	90	313.2(3)	0.54
0.58	*Pnnm*	5.918(3)	7.088(3)	7.437(4)	90	312.0(3)	0.53
0.65	*Pnnm*	5.904(4)	7.082(3)	7.440(4)	90	311.1(3)	0.53
0.88	*Pnnm*	5.865(4)	7.049(4)	7.440(5)	90	307.6(4)	0.56
0.95	*Pnnm*	5.861(5)	7.040(4)	7.451(6)	90	307.4(4)	0.60
1.11	$P2_1/n$	5.814(6)	7.075(13)	7.450(7)	93.14(9)	306.0(7)	0.44
1.28	$P2_1/n$	5.818(7)	7.044(15)	7.445(7)	93.70(9)	304.5(8)	0.50
1.43	$P2_1/n$	5.766(5)	7.002(4)	7.463(7)	94.33(9)	300.5(4)	0.60
1.62	$P2_1/n$	5.745(6)	6.993(10)	7.492(7)	95.37(9)	299.7(6)	0.55
1.80	$P2_1/n$	5.719(5)	6.941(5)	7.480(5)	95.72(6)	295.5(4)	0.46
2.01	$P2_1/n$	5.676(4)	6.877(5)	7.434(5)	95.85(4)	288.7(4)	0.40
2.24	$P2_1/n$	5.638(4)	6.806(4)	7.382(5)	96.10(5)	281.7(3)	0.45
2.44	$P2_1/n$	5.613(3)	6.763(4)	7.360(5)	96.22(5)	277.7(3)	0.48

6. Variable-pressure X-ray diffraction data of $Cd(dca)_2$

$Cd(dca)_2$ adopts a monoclinic structure (space group $P2_1/n$) at ambient conditions and remains in this phase throughout the measured pressure range of 0.05—2.33 GPa, with no evidence of a transition to the orthorhombic rutile-like phase observed in $Ni(dca)_2$, $Fe(dca)_2$, and $Mn(dca)_2$. The evolution of lattice parameters and unit cell volume with pressure is shown in Figure S11. The bulk modulus, obtained from a second-order Birch--Murnaghan fit, is B_0 = 7.0(3) GPa . This value is substantially lower than the 14.9–18.2 GPa observed for the orthorhombic phases of the Ni, Fe, and Mn analogues. Linear compressibilities along the crystallographic axes are K_a = 42(2) TPa^{-1}, K_b = 28.0(3) TPa^{-1}, and K_c = 22.5(7) TPa^{-1}, all positive, confirming the complete absence of NLC. This is a direct consequence of Cd^{2+} (ionic radius 0.95 Å) exceeding the structural tolerance window for the orthorhombic rutile-like framework, which underpins the wine-rack hinging mechanism responsible for NLC in the Ni, Fe, and Mn analogues.

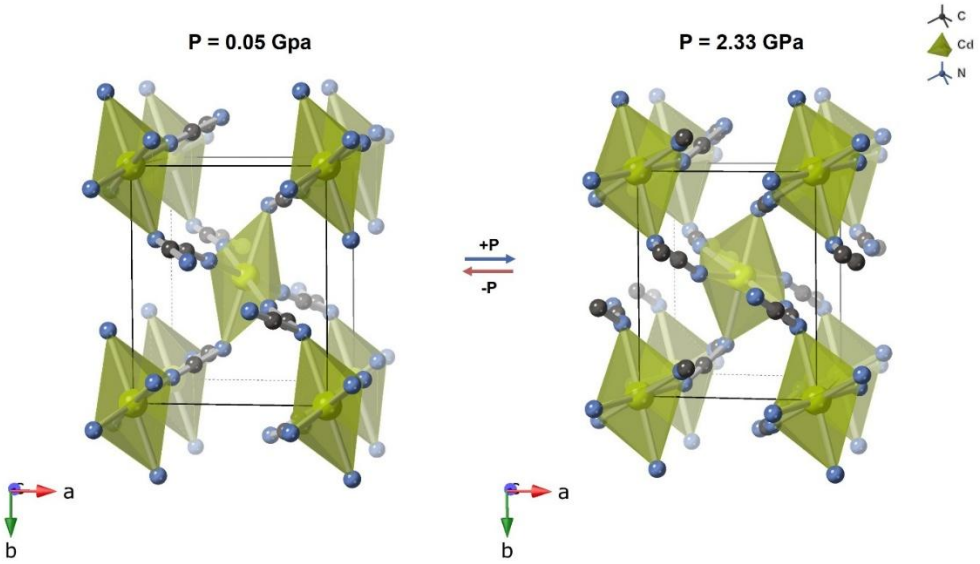

Figure S10: Crystal structures of $Cd(dca)_2$ at 0.05 GPa and 2.33 GPa.

Table S11: Compressibility and bulk modulus of $Cd(dca)_2$

Materials	K_a (Tpa^{-1})	K_b (Tpa^{-1})	K_c (Tpa^{-1})	B_0 (GPa)	B‘	Range (GPa)	Data points
$Cd(dca)_2$	42(2)	28.0(3)	22.5(7)	7.0(3)	6.1(5)	0.05 – 2.33	32

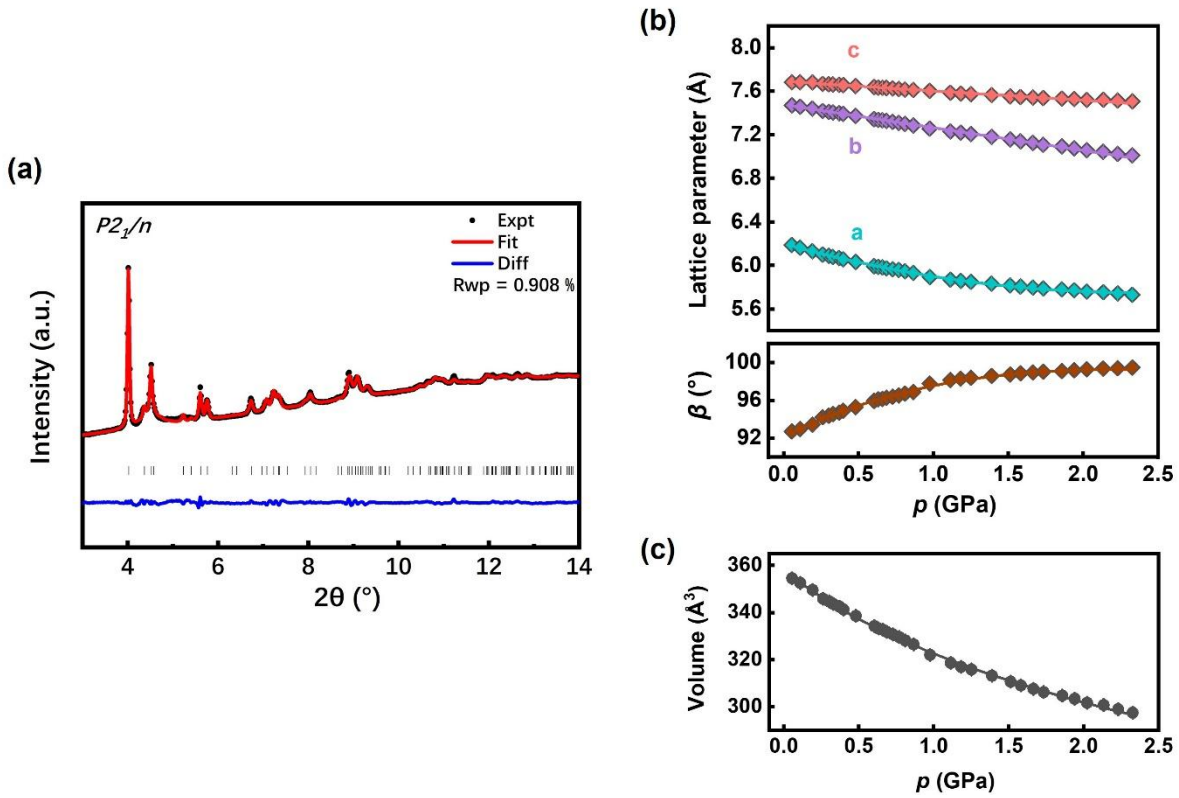

Figure S11. (a) Powder X-ray diffraction pattern of $Cd(dca)_2$ at 0.05 GPa. Data were collected at Diamond Light Source (I15) using radiation with a wavelength of 0.4246 Å. The pattern was fitted using Rietveld refinement. The experimental data are displayed in black, the fit in red, the residuals in grey, and the permitted reflections are denoted by vertical bars. The Rwp value is given as a satisfactory indicator of refinement. (b) Variation of the lattice parameters of $Cd(dca)_2$ as a function of increasing pressure. The parameters a, b and c were all fitted linearly, while the angle β was fitted to a third-order polynomial equation. (c) Volume change of $Cd(dca)_2$ as a function of pressure. All data shown conform to the third-order Birch–Murnaghan equation.